Journal of Power Sources 204 (2012) 155–161

Contents lists available at SciVerse ScienceDirect

Journal of Power Sources

journal homepage: www.elsevier.com/locate/jpowsour

# NiO–graphene hybrid as an anode material for lithium ion batteries

Y.J. Mai, S.J. Shi, D. Zhang, Y. Lu, C.D. Gu, J.P. Tu*

*State Key Laboratory of Silicon Materials and Department of Materials Science and Engineering, Zhejiang University, Hangzhou 310027, China*

ARTICLE INFO

*Article history:*
Received 20 October 2011
Received in revised form
19 December 2011
Accepted 19 December 2011
Available online 29 December 2011

*Keywords:*
Nickel oxide
Graphene
Thermodynamics
Kinetics
Voltage hysteresis

ABSTRACT

A NiO–graphene hybrid is synthesized by a liquid phase deposition method. As an anode material for lithium ion batteries, the cyclic stability and rate capability of NiO is significantly improved after the incorporation of graphene sheets. The NiO–graphene hybrid electrode delivers a capacity of 646.1 mA h $g^{-1}$ after 35 cycles at a current density of 100 mA $g^{-1}$, corresponding to 86.3% capacity retention. When the current density is increased to 400 and 800 mA $g^{-1}$, it still maintains a capacity of 509 and 368.5 mA h $g^{-1}$, respectively. The thermodynamic and kinetic properties of NiO electrodes with and without graphene are investigated by galvanostatic intermittent titration technique. The relationship between the rate and voltage hysteresis is also discussed. The polarization of both the electrodes in all cases obeys ohmic rule in the present rate range. The incorporation of graphene sheets can partly reduce the voltage polarization thereby the voltage hysteresis with increasing the current density. However, the extrapolation to zero current ends up in an approximate residual voltage for both the NiO electrodes.



## 1. Introduction

Since the pioneering work of Tarascon and co-workers on negative-electrode materials of transition metal oxides (TMO) [1,2], many studies have been devoted to optimizing the materials for better electrochemical performances and to trying to overcome those obstacles that keep compounds that electrochemically react with lithium through a conversion reaction far from commercial application [3–6]. Among TMO, NiO is one of the promising anode materials for Li ion batteries because of its high safety, environmental benignity, low cost and outstanding theoretical capacity. However, it still suffers from poor cyclic stability. A variety of appealing strategies have been utilized to overcome this obstacle [7–15]. For example the thin film electrode composed of vertically aligned NiO nanowalls displayed a capacity of 638 mA h $g^{-1}$, with excellent capacity retention of up to 85 cycles at a current density of 1.25 C [16], and the net-structured NiO–C nanocomposite with greatly improved lithium storage capacity in which the amorphous carbon layer significantly enhanced the conductivity of NiO, suppressed the aggregation of active particles and increased the structure stability during the discharge–charge process [17]. Recently, lithium metal alloys [18–20] or metal oxide nanoparticles [21–24] which combined with graphene sheets have been reported to display high specific capacity and excellent cyclic stability as anode materials compared to naked particles. Graphene sheets in the above structure acted as not only a buffer zone of volume variation of the nanoparticles but also a good electron transfer medium.

Another obstacle for, just like other TMO, the application of NiO in commercial devices is strongly handicapped by an unacceptable, in terms of round-trip energy density loss, large voltage hysteresis that is observed between the discharge and charge steps. In fact, the voltage hysteresis is common in both insertion and conversion reaction anodes, and is more visible for the latter. The origins of this hysteresis are far from being understood, but a few studies indicate that it is partly linked to the finite kinetics and another part of this hysteresis has a thermodynamic origin. According to previous reports [25,26], with the help of graphene sheets, NiO electrode shows improved reversible capacity and cyclic performance, however, there is few report on how the introduced graphene sheets affect the thermodynamic and kinetic properties thereby the voltage hysteresis value for NiO electrode.

In this present work, NiO–grpahene hybrid material has been prepared by a liquid phase deposition method, differed from the hydrothermal method of the previous reports [25,26]. In addition, the lithium storage performances including reversible capacity, cyclic stability and rate performance are compared between NiO–grpahene hybrid and bare NiO electrodes. Finally, the voltage hysteresis of both the electrodes associated with the thermodynamic and kinetic reasons are also discussed.

## 2. Experimental

The NiO–graphene hybrid material was prepared as follows. First of all, 0.5 mg $ml^{-1}$ graphite oxide (GO) suspension was

* Corresponding author. Tel.: +86 571 87952856; fax: +86 571 87952573.
*E-mail addresses:* tujplab@zju.edu.cn, tujp@zju.edu.cn (J.P. Tu).

0378-7753/$ – see front matter © 2011 Elsevier B.V. All rights reserved.
doi:10.1016/j.jpowsour.2011.12.038

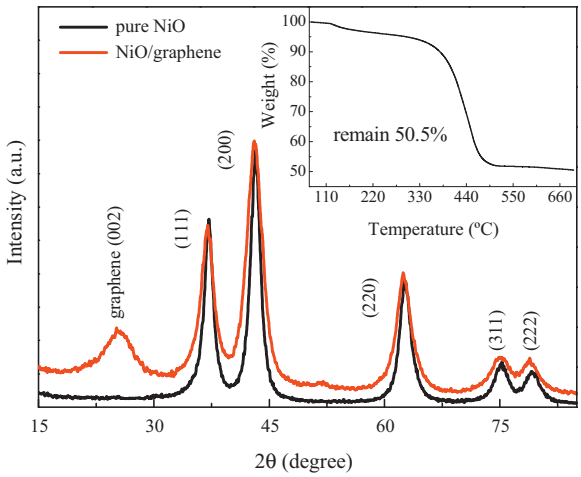


**Fig. 1.** XRD patterns of NiO and NiO–graphene hybrid, and the inset is the TG result of NiO–graphene hybrid.

obtained by sonication. An appropriate amount of $Ni(NO_3)_2{\cdot}6H_2O$, followed by ammonia solution (0.55 M) was slowly added into the above suspension and then stirred for 2 h at room temperature. The precipitation was centrifugalized and washed with distilled water, and dried by freezing drying and then calcined in a tube furnace at 400 °C for 2 h in flowing argon. For comparison, pure NiO was also prepared under the same conditions but without the presence of GO.

The as-prepared materials were characterized by means of X-ray diffraction (XRD, D/max 2550-PC) and transmission electron microscopy (TEM, CM200 and JEOL-2100F). Thermogravimetry (TG, SDT Q600 V8.2 Build 100) analysis from room temperature to 700 °C at a heating rate of 10 °C $min^{-1}$ in air was carried out to estimate the weight percentage of NiO in the hybrid material.

The graphene sheets are also considered as active materials, rather than only act as the conductive additive. So, just like many previous reports [18–24], the same weight percentage of acetylene black is added in both the electrodes. The working electrodes were prepared by a slurry coating procedure. The slurry consisting of 80 wt.% active materials, 10 wt. % acetylene black and 10 wt. % polyvinylidene fluorides dissolved in N-methyl pyrrolidinone were coated on nickel foam with 15 mm in diameter. The electrolyte was 1 M $LiPF_6$ in ethylene carbonate–dimethyl carbonate (1:1 in volume). CR-2025-type coin cells were assembled in a glove box under argon atmosphere. The galvanostatic discharge and charge measurements were conducted on LAND battery program-control test system, in the voltage range of 0.02–3.0 V (vs. $Li/Li^+$) at room temperature (25 ± 1 °C). Galvanostatic intermittent titration technique (GITT) was also performed using LAND battery program-control test system by charging/discharging the cells for 4 h at a rate of C/20 of the theoretical capacity of NiO. The relaxation period was set as 8 h. The electrochemical impedance spectroscopy (EIS) measurements were performed on CHI660C electrochemical workstation over a frequency range of 0.01 Hz–100 kHz by applying an AC signal of 5 mV in amplitude throughout the tests. Before the measurement, the electrodes were cycled for 5 cycles at a current density of 50 mA $g^{-1}$, then discharged to 2.0 V and kept until the open-circuit voltage stabilized.

## 3. Results and discussion

### 3.1. Material characterization

The XRD patterns of pure NiO and NiO–graphene hybrid materials are shown in Fig. 1. All of the diffraction peaks of the powder without graphene can be ascribed to NiO (JCPDS No. 01-073-1519). Compared to the XRD pattern of pure NiO, an additional small and low broad diffraction peak appears at about 25°, corresponding to the (0 0 2) diffraction peak of the disorderedly stacked graphene sheets. These results suggest that the hybrid material is composed of graphene sheets and NiO. The inset is the TG curve of NiO–graphene hybrid, which indicates that the graphene sheets are burn out when the temperature is higher than 500 °C. It is assumed that remaining is NiO and thus the weight percent of NiO in the NiO–graphene hybrid is about 50.5%.

Fig. 2 shows the TEM images of NiO, GO and NiO–graphene hybrid. As shown in Fig. 2a, the flake-like NiO is constructed by many interconnected strips with about 5 nm in width, leaving many interspaces which are about 5 nm in length and 2 nm in width between the strips. Fig. 2b shows the initial GO sheets, which exhibit smooth surfaces. It is noticed that the central part of GO sheets are homogeneous and featureless region, whereas the edges trend to scroll and the wrinkled morphology is more obvious. However, the smooth surfaces of the pristine GO sheets are homogeneously anchored by many nanoparticles for the NiO–graphene hybrid, as shown in Fig. 2c. The graphene sheets are comprised of 3–5 individual graphene and the NiO nanoparticles obtained are up to several nanometers in sizes and are well crystallized (Fig. 2d). Some of them show clear lattice fringes and the strip distance is about 0.24 nm, closed to *d*-value of (1 1 1) plane of NiO. In order to better understand the effect of the microstructure of NiO–graphene hybrid on its electrochemical performance, the hybrid electrode after 35 cycles at a current density of 100 mA $g^{-1}$ is also investigated by TEM. Fig. 2e reveals the disintegration of the initial particles into smaller NiO nanoparticles. However, they are still anchored on graphene sheets and no obvious aggregation of nanoparticles is observed despite that they have undergone 35 times of volume expansion/contraction associated with the lithium insertion and extraction process, highlighting the structure stability of NiO–graphene hybrid electrode. It is purposed that the capacity decay could be attributed to the loss of the electrical contact of active particles owing to large volume variation and microstructure instability as a consequence of phase transformation reaction during the lithium uptake and extraction [17,27]. The unique microstructure of the hybrid in which the well-crystallized NiO nanoparticles homogeneously anchored on good mechanical flexibility graphene sheets results in a stronger endurance to volume variation and stops active particles from aggregating. Also, conducting graphene enables fast electron transport during discharge and charge process. Therefore, it is expected that the NiO–graphene hybrid will display excellent cycling performance and rate capability.

### 3.2. Electrochemical performance

Fig. 3a compares the cyclic performance of pure NiO and NiO–graphene hybrid electrodes. The reversible capacity of pure NiO continuously decays on cycling, which is similar to the previous reports [1,28–30]. It can be seen that the reversible capacity of pure NiO electrode decreases from 720.9 to 289.3 mA h $g^{-1}$ after 35 cycles at a current density of 100 mA $g^{-1}$, corresponding to 40.1% capacity retention. In contrast, the reversible capacity of the NiO–graphene hybrid electrode slightly decreases in the first 5 cycles and after that it keeps a stable value and reaches a value of 646.1 mA h $g^{-1}$ after 35 cycles, corresponding to 86.3% capacity retention.

Another advantage of the NiO–graphene hybrid electrode is its rate performance (Fig. 3b). The reversible capacity of NiO–graphene hybrid electrode is stable at ca. 600 mA h $g^{-1}$ after 10 cycles at a current density of 200 mA $g^{-1}$. Upon increasing the current density to 400 and 800 mA $g^{-1}$, its reversible capacities are still maintained

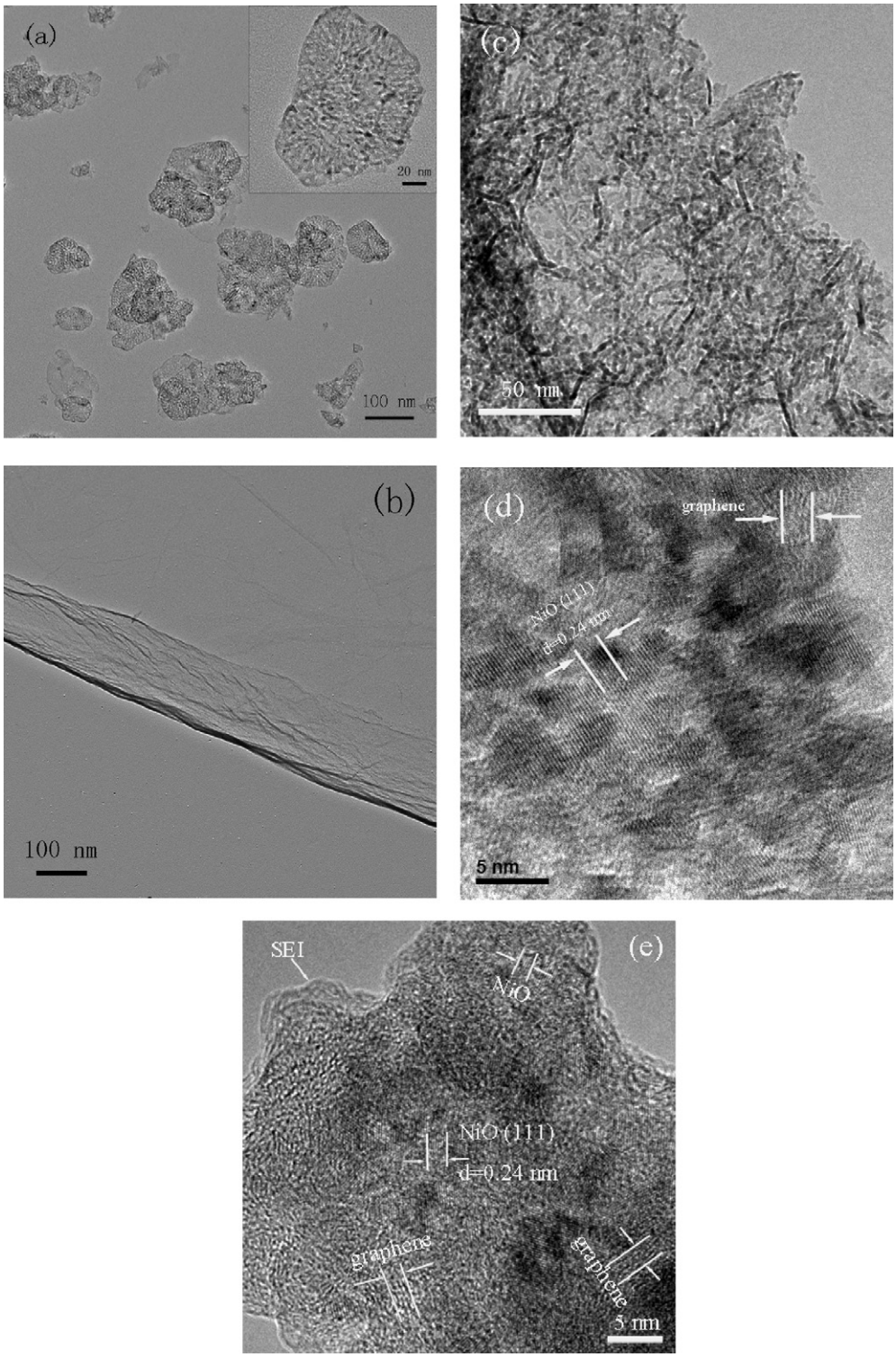


**Fig. 2.** Low magnification TEM image of NiO (a), GO (b) and NiO–graphene hybrid (c) and high magnification TEM image of NiO (the inset in Fig. 2a), NiO–graphene hybrid (d) before and (e) after 35 cycles of discharge/charge.

at ca. 509 and 368.5 mA h $g^{-1}$, corresponding to 73.6% and 53.3% capacity retention of the first capacity, respectively. When the current density returns to the initial 200 mA $g^{-1}$ after 40 cycles, the NiO–graphene hybrid recovers 78.8% of its first capacity, indicating the stable structure of the electrode. These performances are remarkably superior to that of pure NiO electrode, for example, when the current density is 800 mA $g^{-1}$ and returns to the initial 200 mA $g^{-1}$ after 40 cycles, its reversible capacity are 56.2 and 128.9 mA h $g^{-1}$ corresponding to only 8.7% and 20% capacity retention of the first capacity. As expected, enhancement of the electronic conductivity is effect to improve the rate performance of electrodes. Fig. 3c shows the EIS of pure NiO and NiO–graphene hybrid electrodes. Two depressed semicircles are observed for both the electrodes, including the one located in high frequency

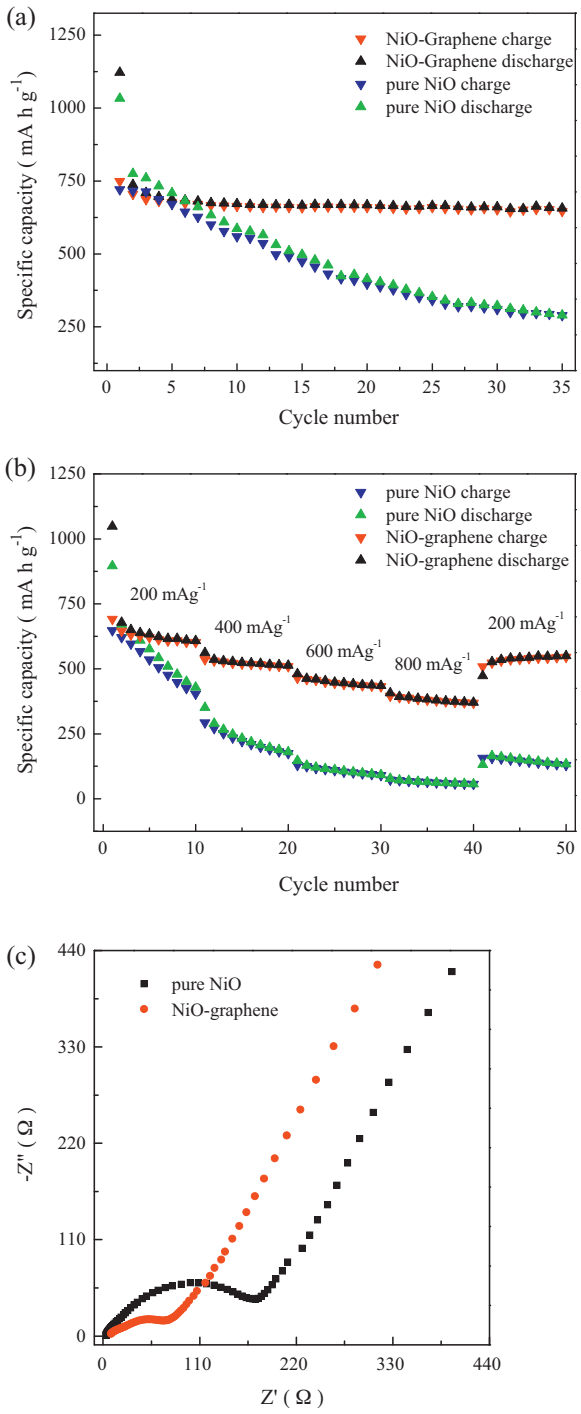


**Fig. 3.** (a) Cyclic stability at a current density of 100 mA g$^{-1}$, (b) rate capability and (c) EIS results of NiO and NiO–graphene hybrid electrodes.

ranges assigned to surface film resistance and the one located in medium frequency ranges assigned to charge transfer impedance [17,31]. Obviously, the diameter of the second semicircle for the NiO–graphene hybrid is smaller than that of pure NiO, revealing lower charge transfer impedance. This phenomenon indicates that the electronic conductivity of NiO is improved after the incorporation of graphene sheets because the graphene sheets are good electronic conductor which can keep good electronic wetting of the anchored NiO nanoparticles. Also, it is worth mentioning that the above lithium storage performance is not superior to mesoporous carbon-encapsulated NiO nanocomposite [8] or highly ordered mesoporous NiO [32], but is a significant improvement compared to previous reports [17,26,29,33,34].

### 3.3. Thermodynamic and kinetic properties

The overall Li uptake and Li extraction from NiO can be writhen as:

$$NiO + 2Li^+ + 2e \leftrightarrow Ni + Li_2O \quad (1)$$

If the reactant and the product are perfect bulk materials, taking no account for the polarization, the above conversion reaction should correspond to a plateau in voltage profile with a capacity of 718 mA h g$^{-1}$ at the electromotive force (emf) of 1.945 V (vs. Li/Li$^+$), which can be calculated using the Nernst equation [35]:

$$\Delta G = \Delta G_f^\circ(Li_2O) - \Delta G_f^\circ(NiO) = -2EF \quad (2)$$

As shown in Fig. 4a, the first discharge voltage-specific capacity curve of NiO electrode exhibits three distinct sloping voltage ranges. Given to NiO electrode does not exhibit a solid solution domain prior to the conversion process, the capacity above plateau voltage can be attributed to the reduction of electrolyte and the formation of SEI film. The large plateau capacity at about 0.6 V (vs. Li/Li$^+$) corresponds to the conversion reaction from initial bulk NiO to Ni/$Li_2O$ nanocomposite. The low-voltage capacity is nested in either the pseudocapacitive character of the in situ made polymeric/gel film [36] or an interfacial mechanism, which has been explained by Maier et al. [37–39], where excess lithium are accommodated in the phase boundary regions via charge separation between nanosized Ni and $Li_2O$. The behavior of the NiO–graphene hybrid is similar to the NiO electrode (Fig. 4b). In addition, since the conversion reaction from NiO to Ni/$Li_2O$ nanocomposite occurs below the emf value of 1.945 V (vs. Li/Li$^+$), whereas reverse conversion reaction from the Ni/$Li_2O$ to NiO occurs above the emf in the real electrode reaction because of polarization, the discharge plateau at about 0.6 V and the average charge plateau about 2.25 V in the first cycle, corresponds to the reduction and oxidation of NiO, respectively, as shown in Eq. (1). Therefore, the lithium uptake/extraction capacities at the plateau regions during the first cycle calculated from the GITT curves can reflect the utilization of NiO active material, ignoring the capacity contribution of SEI and low voltage area. For clarity, these capacities are listed in Table 1. It can be seen that the NiO electrode delivers a plateau capacity of 704.8 mA h g$^{-1}$ for the first discharge, which is closed to the theoretic capacity of 718 mA h g$^{-1}$, indicating the full lithium uptake. In the subsequent charging, it displays a plateau capacity of 539.1 mA h g$^{-1}$, corresponding to an initial coulombic efficiency of 76.5% if the initial coulombic efficiency is defined as the rate of the first charge plateau capacity to the first discharge plateau capacity of NiO. For the NiO–graphene hybrid electrode, the first discharge plateau capacity and charge plateau capacity are 367.3 and 321.5 mA h g$^{-1}$, respectively. However, in the NiO–graphene hybrid, the weight percent of NiO is 50.5% as demonstrated by TG analysis (the inset in Fig. 1). This means the theoretic plateau capacity of the NiO–graphene hybrid electrode is 362.6 mA h g$^{-1}$. Therefore, the hybrid electrode is also full lithiation for the first discharge, but the initial coulombic efficiency is 87.5%, which is higher than that of bare NiO, suggesting a better utilization of NiO active material for the hybrid electrode.

The difference estimated from the GITT curve between the cut-off voltage and the open circuit voltage measured after relaxation for both the electrodes is shown in Fig. 4c, in which 0 refers to full delithiation state and 1 refers to full lithiation state. Such difference can roughly reflect the polarization and this polarization changes a litter with lithium insertion but continuously increases with the lithium extraction. In term of electronic conductivity, the above trend of polarization can be explained by the fact that in the case

**Table 1**
The lithium uptake/extraction capacities at the plateau regions during the first cycle calculated from the GITT curves.

| Electrodes | NiO | NiO–G | Electrodes | NiO | NiO–G |
|---|---|---|---|---|---|
| 1st $D_{plateau}$ (mA h g$^{-1}$) | 704.8 | 367.3 | 1st $C_{plateau}$ (mA h g$^{-1}$) | 539.1 | 321.5 |
| 1st $D_{slope}$ (mA h g$^{-1}$) | 548.5 | 487.8 | 1st $C_{slope}$ (mA h g$^{-1}$) | 548.5 | 487.8 |
| 1st $D_{total}$ (mA h g$^{-1}$) | 1540.4 | 1182.1 | 1st $C_{total}$ (mA h g$^{-1}$) | 1087.6 | 809.3 |
| Slope voltage range for discharge (V) | 0.6–0 | 0.6–0 | Slope voltage range for charge (V) | 0–1.945 | 0–1.945 |

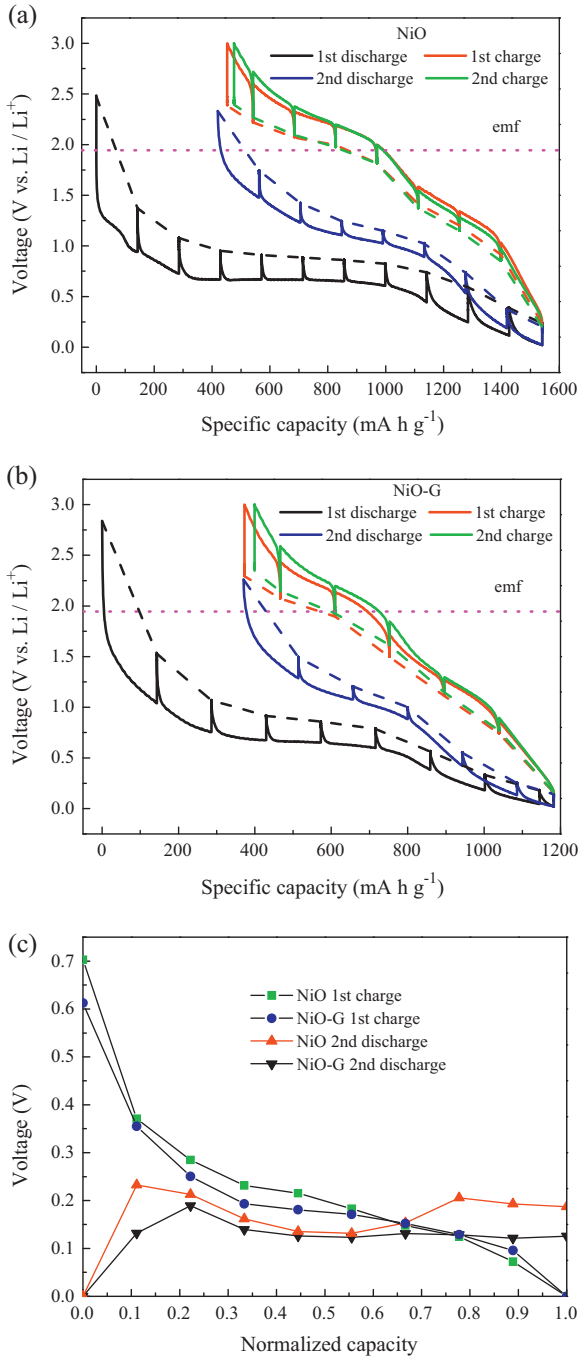


**Fig. 4.** GITT curves of NiO (a) and NiO–graphene hybrid electrode (b). Solid lines are GITT result, dash lines are open circuit voltage and dot dash lines are the emf value. (c) The difference estimated from the GITT curve between the cutoff voltage and the open circuit voltage was measured after relaxation.

of lithium uptake, a continuous increase in electronic conductivity is expected since insulating NiO nanoparticles are transferred into nickel nanoparticles. Sauvage et al. [40] have demonstrated the electronic conductivity of Ni/$Li_2O$ composite is as high as 5000 S cm$^{-1}$ after 2/3 of the transition completion due to the Ni nanoparticle percolation within the $Li_2O$ matrix. In contrast, in the case of lithium extraction, the electronic conduction is expected to become increasingly problematic because of the expense of nickel metal to the formation of NiO nanoparticles. It is noticed that the introduction of graphene has result in a small reduction of polarization at the present rate of as low as 1/20 C, however, as shown in the following section, when the rate is increased to some extent, the NiO–graphene hybrid electrode shows an obvious decreased polarization.

Voltage hysteresis of electrode materials refers to the phenomenon that discharge potential is lower than charge potential [31]. Different reasons lead to different polarizations during discharge/charge process, and the total polarization results in the voltage hysteresis. The voltage hysteresis produces a huge round-trip inefficiency, resulting in a barrier between laboratory and society as the associated energy losses would make a battery unviable [5,41]. To be sure, the mechanism of lithium storage for graphene sheets is different from NiO which stores lithium by the conversion reaction. The lithium is stored by intercalating into the graphene sheets which are stacked in a roughly parallel fashion [42,43], and a faradic capacitance associated with their edge planes, vacancies and adsorbed functional groups [44,45]. However, the voltage hysteresis curve is the sum of the polarization of both charging and discharging at galvanostatic mode and can be used to reflect the kinetic property of different electrode materials storing lithium by different mechanisms. It is obtained by subtracting the discharge curve at the second cycle from the charge curve at the first cycles after normalization. For the capacity normalization used here, 0 refers to full delithiation state charged to 3.0 V and 1.0 means starting of charging. As shown in Fig. 5a, the voltage polarization of NiO electrode is about 0.5–1.0 V in all lithiation/delithiation range. Compared to the NiO electrode, the NiO–graphene hybrid exhibits a slight reduction of voltage polarization. Interestingly, the overall voltage polarization of graphene sheets electrode is obviously reduced after the incorporation of NiO and the voltage hysteresis curve of the NiO–graphene hybrid exhibits the same characters as the pure NiO electrode although the weight percent of graphene in the obtained hybrid is as high as 49.5%. A possible reason is that the reduced graphene sheets contain many dangling bonds, surface defects and vacancies, which are considered as the active sites for the formation of SEI or banding with lithium. The kinetics of lithium intercalation is limited by the thick SEI film because all lithium ions in an electrolyte solution must cross this film before the formation of the lithium-intercalation graphite compounds. Also, the banding between active sites and lithium would be the activated processes, which can lead to hysteresis. The anchored NiO nanoparticles cover and remove some active sites, leading to an obvious reduction of voltage polarization. However, in the hybrid material, the voltage polarization resulting from NiO is more obvious compared with the graphene sheets modified by NiO nanoparticles and thus the voltage polarization of NiO dominates the whole charge/discharge process of NiO–graphene electrode.

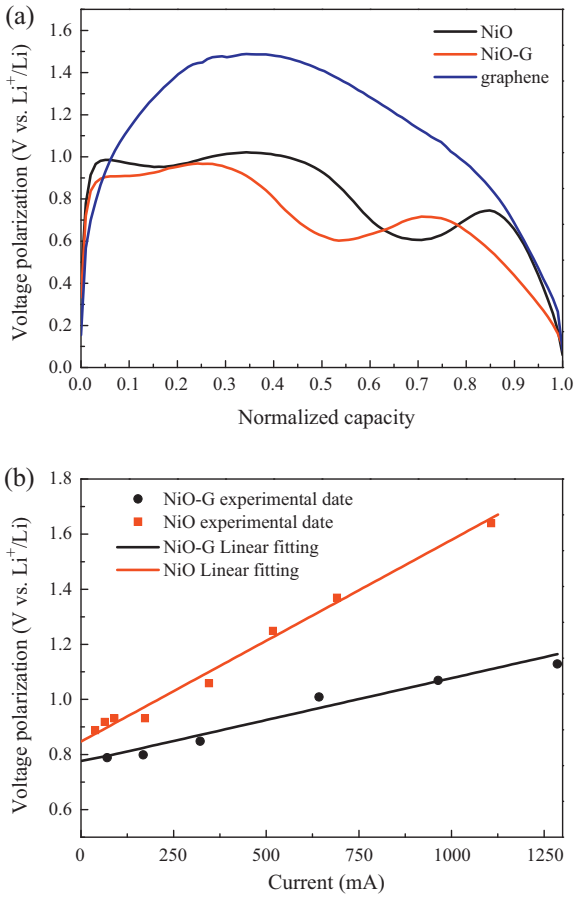


**Fig. 5.** (a) Comparison of voltage hysteresis curves of NiO, graphene thermal reduced from GO at 400 °C and NiO–graphene hybrid electrode at a current density of 100 mA $g^{-1}$ and (b) the variation of voltage polarization as a function of current of NiO and NiO–graphene hybrid electrodes.

Fig. 5b displays the variation of voltage polarization as a function of current for the NiO and NiO–graphene hybrid electrodes. The polarization values were extracted from the middle of the sloppy plateau. It can be seen that, a quasi-linear correlation between the polarization value and applied current is noted for both the electrodes, suggesting that the electrode polarization in all cases obeys ohmic rule in the present rate range. In addition, as expected, the polarization values increase with the increase of rate for both the electrodes, however, the upward trend is more obvious for the NiO electrode than that for the NiO–graphene hybrid. This indicates the polarization associated with the conversion reason of NiO is reduced with the corporation of graphene, which can be mainly attributed to the increased electronic conductivity of NiO in the hybrid electrode. Interestingly, if the polarization resulting from the electronic transport or/and mass transport is the only source of voltage hysteresis, the polarization value should become vanishingly small when the applied current is reduced to a sufficiently small value. However, the extrapolation to zero current ends up in an approximate residual voltage for both the electrodes, for example 0.78 V for the NiO–graphene hybrid and 0.85 V for the NiO electrode. Recent reports point out the origin of this zero-current polarization is very likely related to thermodynamic factor. Gaberscek et al. [46] presented the thermodynamic origin of this zero-current polarization in insertion batteries by the many particle effect; Wang and Zhu [31] attributed this value of $LiFePO_4$ to the strain accommodation energy of phase transformation; and Li et al. [47] explained this polarization value of MnO electrode in the term of energy difference induced by volume variation and surface energy. Like MnO, NiO is directly conversed, without any solid solution domain, to metallic particles when it reacts with lithium. Therefore the volume variation and surface energy is also assigned to the origin of the zero-current polarization. However, this value is only 0.3 V for silicon electrode [6], which exhibits as large as 300% volume variation. So, whether the energy difference induced by volume variation and surface energy is the only reason for the zero-current polarization is not clear and more thermodynamic date are needed.

## 4. Conclusions

The NiO–graphene hybrid is synthesized in which NiO nanoparticles are up to several nanometers in sizes and homogeneously anchored on conducting graphene sheets. As active material for Li ion batteries, the cyclic stability and rate capability of NiO are significantly improved by the incorporation of graphene because of establishment of good electronic contact between active particles and fast electron transport during discharge-charge process. The NiO–graphene hybrid delivers a capacity of 646.1 mA h $g^{-1}$ after 35 cycles at a current density of 100 mA $g^{-1}$, corresponding to 86.3% capacity retention. When the current density is increased to 400 and 800 mA $g^{-1}$, it still can deliver a capacity of 509 and 368.5 mA h $g^{-1}$, respectively. The incorporation of graphene can partially decrease the voltage polarization, especially when the hybrid electrode is discharged and charged at a high rate, however, it has a slight effect on the zero-current polarization.

## References

[1] P. Poizot, S. Laruelle, S. Grugeon, L. Dupont, J.M. Tarascon, Nature 407 (2000) 496–499.
[2] A. Debart, L. Dupont, P. Poizot, J.B. Leriche, J.M. Tarascon, J. Electrochem. Soc. 148 (2001) A1266–A1274.
[3] D.W. Liu, G.Z. Cao, Energy Environ. Sci. 3 (2010) 1218–1237.
[4] P. Bruce, B. Scrosati, J.M. Tarascon, Angew. Chem. Int. Ed. 47 (2008) 2930–2946.
[5] J. Cabana, L. Monconduit, D. Larcher, M.R. Palacin, Adv. Mater. 22 (2010) E170–E192.
[6] H. Li, Z.X. Wang, L.Q. Chen, X.J. Huang, Adv. Mater. 21 (2009) 4593–4607.
[7] E. Hosono, S. Fujihara, I. Honma, H. Zhou, Electrochem. Commun. 8 (2006) 284–288.
[8] M.Y. Cheng, B.J. Hwang, J. Power Sources 195 (2010) 4977–4983.
[9] M.F. Hassan, M.M. Rahman, Z.P. Guo, Z.X. Chen, H.K. Liu, J. Mater. Chem. 20 (2010) 9707–9712.
[10] X.H. Huang, J.P. Tu, X.H. Xia, X.L. Wang, J.Y. Xiang, Electrochem. Commun. 10 (2008) 1288–1290.
[11] Y.J. Mai, J.P. Tu, X.H. Xia, C.D. Gu, X.L. Wang, J. Power Sources 196 (2011) 6388–6393.
[12] X.H. Huang, J.P. Tu, X.H. Xia, J.Y. Xiang, X.L. Wang, J. Power Sources 195 (2010) 1207–1210.
[13] C.H. Xu, J. Sun, L. Gao, J. Power Sources 196 (2011) 5138–5142.
[14] X.H. Huang, J.P. Tu, X.H. Xia, X.L. Wang, J.Y. Xiang, L. Zhang, Y. Zhou, J. Power Sources 188 (2009) 588–591.
[15] X.H. Wang, Z.B. Yang, X.L. Sun, X.W. Li, D.S. Wang, P. Wang, D.Y. He, J. Mater. Chem. 21 (2011) 9988–9990.
[16] B. Varghese, M.V. Reddy, Z. Yanwu, C.S. Lit, T.C. Hoong, G.V. Subba Rao, B.V.R. Chowdari, A.T.S. Wee, C.T. Lim, C.-H. Sow, Chem. Mater. 20 (2008) 3360–3367.
[17] X.H. Huang, J.P. Tu, C.Q. Zhang, J.Y. Xiang, Electrochem. Commun. 9 (2007) 1180–1184.
[18] H.F. Xiang, K. Zhang, G. Ji, J.Y. Lee, C.J. Zou, X.D. Chen, J.S. Wu, Carbon 49 (2011) 1787–1796.
[19] G.X. Wang, B. Wang, X.L. Wang, J. Park, S.X. Dou, H. Ahn, K. Kim, J. Mater. Chem. 19 (2009) 8378–8384.
[20] X.Y. Wang, X.F. Zhou, K. Yao, J.G. Zhang, Z.P. Liu, Carbon 49 (2011) 133–139.
[21] G.M. Zhou, D.W. Wang, F. Li, L.L. Zhang, N. Li, Z.S. Wu, L. Wen, G.Q. Lu, H.M. Cheng, Chem. Mater. 22 (2010) 5306–5313.
[22] B. Wang, X.L. Wu, C.Y. Shu, Y.G. Guo, C.R. Wang, J. Mater. Chem. 20 (2010) 10661–10664.
[23] Z.-S. Wu, W. Ren, L. Wen, L. Gao, J. Zhao, Z. Chen, G. Zhou, F. Li, H.-M. Cheng, ACS Nano 4 (2010) 3187–3194.
[24] Y.J. Mai, X.L. Wang, J.Y. Xiang, Y.Q. Qiao, D. Zhang, C.D. Gu, J.P. Tu, Electrochim. Acta 56 (2011) 2306–2311.
[25] Y.Q. Zou, Y. Wang, Nanoscale 3 (2011) 2615–2620.
[26] I.R.M. Kottegoda, N.H. Idris, L. Lu, J.-Z. Wang, H.-K. Liu, Electrochim. Acta 56 (2011) 5815–5822.
[27] J.Y. Xiang, J.P. Tu, Y.F. Yuan, X.L. Wang, X.H. Huang, Z.Y. Zeng, Electrochim. Acta 54 (2009) 1160–1165.

[28] X.H. Huang, J.P. Tu, Y.Z. Yang, J.Y. Xiang, Electrochem. Commun. 10 (2008) 16–19.
[29] L. Liu, Y. Li, S.M. Yuan, M. Ge, M.M. Ren, C.S. Sun, Z. Zhou, J. Phys. Chem. C 114 (2010) 251–255.
[30] M.M. Rahman, S.-L. Chou, C. Zhong, J.-Z. Wang, D. Wexler, H.-K. Liu, Solid State Ionics 180 (2010) 1646–1651.
[31] Y.J. Zhu, C.S. Wang, J. Power Sources 196 (2011) 1442–1448.
[32] H. Liu, G.X. Wang, J. Liu, S.Z. Qiao, H. Ahn, J. Mater. Chem. 21 (2011) 3046–3052.
[33] L. Yuan, Z.P. Guo, K. Konstantinov, P. Munroe, H.K. Liu, Electrochem. Solid State Lett. 9 (2006) A524–A528.
[34] X.H. Huang, J.P. Tu, Z.Y. Zeng, J.Y. Xiang, X.B. Zhao, J. Electrochem. Soc. 155 (2008) A438–A441.
[35] H. Li, P. Balaya, J. Maier, J. Electrochem. Soc. 151 (2004) A1878–A1885.
[36] S. Laruelle, S. Grugeon, P. Poizot, M. Dolle, L. Dupont, J.M. Tarascon, J. Electrochem. Soc. 149 (2002) A627–A634.
[37] P. Balaya, H. Li, L. Kienle, J. Maier, Adv. Funct. Mater. 13 (2003) 621–625.
[38] Y.F. Zhukovskii, E.A. Kotomin, P. Balaya, J. Maier, Solid State Sci. 10 (2008) 491–495.
[39] J. Maier, Nat. Mater. 4 (2005) 805–815.
[40] F. Sauvage, J.M. Tarascon, E. Baudrin, J. Phys. Chem. C 111 (2007) 9624–9630.
[41] P.L. Taberna, S. Mitra, P. Poizot, P. Simon, J.M. Tarascon, Nat. Mater. 5 (2006) 567–573.
[42] Y.H. Liu, J.S. Xue, T. Zheng, J.R. Dahn, Carbon 34 (1996) 193–200.
[43] J.R. Dahn, T. Zheng, Y. Liu, J.S. Xue, Science 270 (1995) 590–593.
[44] S.B. Yang, X.L. Feng, L.J. Zhi, Q.A. Cao, J. Maier, K. Mullen, Adv. Mater. 22 (2010) 838–842.
[45] A.V. Murugan, T. Muraliganth, A. Manthiram, Chem. Mater. 21 (2009) 5004–5006.
[46] W. Dreyer, J. Jamnik, C. Guhlke, R. Huth, J. Moskon, M. Gaberscek, Nat. Mater. 9 (2010) 448–453.
[47] K.F. Zhong, B. Zhang, S.H. Luo, W. Wen, H. Li, X.J. Huang, L.Q. Chen, J. Power Sources 196 (2011) 6802–6808.